RESEARCH PAPER

Corrosion and Bioactivity Properties of Calcium-Phosphate PEO Coating on AZ31 Mg Alloy Reinforced by Forsterite (Mg$_2$SiO$_4$) Nanoparticles

Amirhossein Kazemi, Arash Fattah-alhosseini*, Maryam Molaei, Meisam Nouri

* a.fattah@basu.ac.ir

Department of Materials Engineering, Bu-Ali Sina University, Hamedan 65178-38695, Iran

Abstract: *In this study, for the first time, the Forsterite (Mg$_2$SiO$_4$) nanoparticles (NPs) with the size of about 25 nm were added to the phosphate-based electrolyte, and the characteristics and properties of the obtained plasma electrolytic oxidation (PEO) coating on AZ31 Mg alloy was investigated. The results of the potentiodynamic polarization measurements revealed that after one week of exposure to simulated body fluid (SBF) solution, the coating with Mg$_2$SiO$_4$ NPs possessed 12.30 kΩ cm^2 polarization resistance, which was more than two times greater than that of the coating without NPs. The thicker coating layer, lower wettability, and also presence of Mg$_2$SiO$_4$ NPs inside the pores were responsible for enhanced corrosion protection in the Mg$_2$SiO$_4$ NPs incorporated coating. After three weeks of immersion in SBF solution, the in-vitro bioactivity test results indicated the ability of the NPs-containing coating to form apatite (Ca/P ratio of 0.92) was weaker than the coating without NPs (Ca/P ratio of 1.17). This could be attributed to the lower wettability of the coating with NPs and supports that the addition of the nanoparticles is not beneficial to the bioactivity performance of the coating.*

Keywords: AZ31 Mg alloy, plasma electrolytic oxidation (PEO), Forsterite (Mg$_2$SiO$_4$), corrosion; bioactivity.

1. INTRODUCTION

Mg has become an exciting candidate for cardiovascular stents and musculoskeletal systems implants due to its good biodegradability, proximity of its elastic modulus to the elastic modulus of bone, and decreased stress-shielding behavior. Using of Mg for internal load-bearing devices eliminates the need for a second surgery to remove the implant, saving the patient money and alleviating their discomfort. However, chemically complex physiological environments that include Cl$^-$ ions can accelerate the degradation rate of Mg due to its high chemical activity. Early rapid decomposition of Mg releases a substantial amount of H$_2$ gas and causes subsequent quick gas evolution and elevated pH in the alkaline environment, which leads to injury in the tissue at the vicinity of the implant and also a reduction in its mechanical strength. Therefore, enhancing the corrosion resistance of Mg-based implants is a critical issue that should be addressed to overcome the clinical limitations of these implants [1–5].

To increase the corrosion protection of Mg-based implants, different surface modification methods have been investigated which can be categorized into three main groups: chemical, physical, and physico-chemical [6]. The PEO treatment is an electrochemical surface process for fabricating well-adhered thick ceramic oxide coatings on Mg and its alloys surface to increase their resistance against corrosion [7–9]. PEO procedure commonly happens in alkaline electrolytes and involves anodizing at potentials above the dielectric breakdown of the conventional anodic oxide layer. The breakdown is characterized by the motion of several quick micro-discharges over the surface of the bare metal [10, 11]. As one of the most significant benefits of the PEO process, the in-situ addition of nanoparticles (NPs) into the base electrolytes can significantly improve the structure and corrosion performance of PEO coatings [12–14]. Concentration, size, zeta potential, and the melting point of the NPs are the most important parameters influencing the coatings qualities [15].

Forsterite (Mg$_2$SiO$_4$) is a suitable candidate for bone implant applications due to its promising biocompatibility, corrosion resistance, and mechanical properties [16–20]. Mg$_2$SiO$_4$ can be decomposed into silicon (Si) which is a trace element in the composition of bone and encourages the proliferation and adhesion of osteoblast cells [21, 22].

As far as the authors know, up to now, Mg$_2$SiO$_4$-based PEO coatings on Mg and its alloys have been obtained only through using silicate-based

Amirhossein Kazemi, Arash Fattah-alhosseini, Maryam Molaei, Meisam Nouri

electrolytes [23–25]. It has been reported that the presence of the Mg_2SiO_4 phase due to its high inertness, can increase the corrosion resistance of PEO coatings [20, 26–30]. Moreover, the Mg_2SiO_4 phase in PEO coatings may act as the nucleation site for apatite precipitation which can increase the bioactivity [31]. In the present work and for the first time, synthesized Mg_2SiO_4 NPs were successfully incorporated into the Ca-P PEO coatings on AZ31 alloy. The surface characteristics of the as-prepared coatings, including roughness and wettability, corrosion behavior, and bioactivity properties, as well as structure and composition, were examined to study how Mg_2SiO_4 NPs addition can influence those properties and whether Mg_2SiO_4 NPs can be as effective as Mg_2SiO_4 phase formed by silicate-based electrolyte or not.

2. EXPERIMENTAL PROCEDURE

2.1. Synthesis of Mg_2SiO_4 NPs

The Mg_2SiO_4 NPs were produced through mechanical alloying technique using a mechanical milling machine. For this purpose, magnesium oxide (MgO) and silicon dioxide (SiO_2) particles, both with the size of 20 nm, were combined with specific stoichiometric ratios in zirconium dioxide (ZrO_2) cups for 10 hours at a rotating speed of 500 rpm. After removing the obtained mixture from the milling machine, it was sintered at a temperature of 1200°C. Finally, the size and composition of the obtained Mg_2SiO_4 particles were evaluated using FE-SEM (QUANTA 200 FEI) and X-ray diffraction technique (XRD, with Cu Kα radiation at a scan range of 10-80º, ASENWARE, AW-XDM300), respectively (Fig. 1). The average size of Mg_2SiO_4 particles was measured as 25 nm. A zeta potential analyzer (Zetasizer Nano ZS ZEN 3600, Malvern) was employed to measure the zeta potential of the Mg_2SiO_4 particles in the electrolyte.

2.2. PEO coatings preparation

Rectangular-shaped pieces of AZ31 Mg alloy (with dimensions of $15 \times 20 \times 3$ mm^3) were used as the substrate. The chemical composition of AZ31 alloy and the detailed description of the PEO coating process can be found in our previous publication [32]. The PEO coating process was performed in the phosphate-based electrolyte containing 5 g/l $Na_3PO_4.12H_2O$, 3 g/l KOH, 1 g/l $Ca_3(PO_4)_2$, without and with 3 g/l Mg_2SiO_4 NPs. To disperse Mg_2SiO_4 particles in the electrolyte, the prepared electrolyte was mixed in an ultrasonic mixer for one hour. The PEO processes were executed at 12 A/dm^2 current density, 1 kHz frequency, 50 % duty cycle, and for 6 minutes.
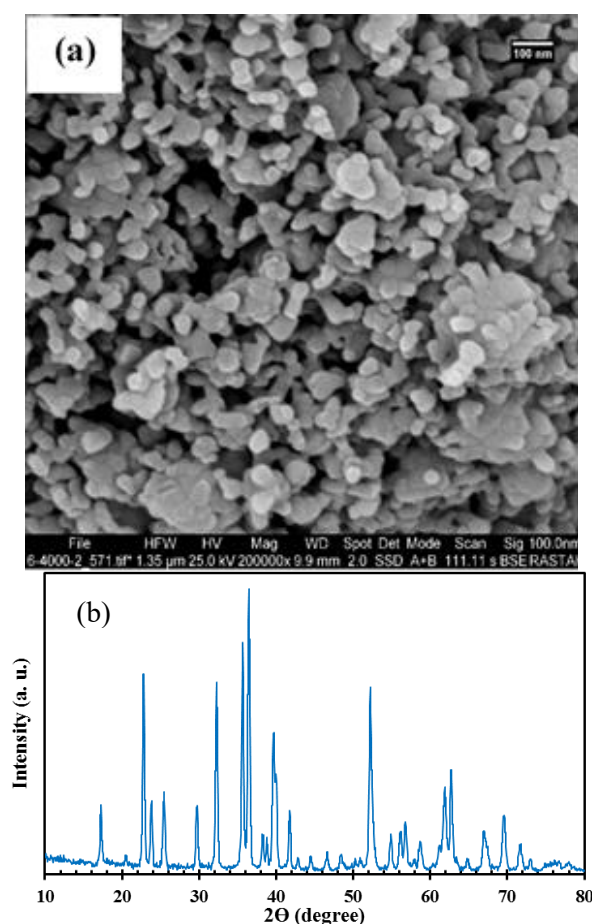
Fig. 1. (a) FE-SEM image at a magnification of 200000x and (b) XRD pattern of Mg_2SiO_4 NPs.

2.3. Coatings characterizations

The surface microstructure and elemental analysis of coatings were studied by FE-SEM (QUANTA FEG 450) equipped with an EDS detector (EDAX OCTANE ELITE). The cross-sectional micrographs were captured by SEM (JSM-840) and the thickness of the coatings was measured with the help of ImageJ software. Phase analysis of coatings was studied with an XRD (PHILIPS-PW1730) operating at 40 kV and 30 mA using Cu Kα radiation at the 2Θ range of 10º to 80º and the FT-IR (Tensor 27 BRUKER) in the transmission from 600 to 4000 cm^{-1}. To determine the surface roughness of the coatings,

2

a roughness tester (Mahr GmbH. Gottingen, M300-RD18) was utilized. For each coating, the tests were executed at five different regions and the average value was reported. Wettability measurements were conducted using distilled water droplets and a contact angle goniometer, following the sessile drop method (CA-500 equipped with a Dino-lite camera, Iran). Five measurements were done for each sample and the mean value was calculated.

2.4. Coatings corrosion properties

The corrosion behavior of coatings was investigated using electrochemical impedance spectroscopy (EIS) and potentiodynamic polarization (PDP) techniques in simulated body fluid (SBF) solutions with a pH of 7.4 at 37 ± 0.5ºC. The chemical ingredients of the SBF solution are summarized in Table 1 [33]. A detailed description of EIS measurements can be found in ref. [32].
EIS measurements were conducted after exposure for 1 hour, 1 day, 3 days, and 1 week to the solution. After 1 week, the PDP tests were conducted from −0.250 V below the open circuit potential (OCP) values with a scan rate of 0.001 V/s. Then, the surface of coatings was analyzed utilizing FE-SEM and EDS techniques. Each measurement was repeated three times to ensure the accuracy of the results.

2.5. Coatings in-vitro bioactivity behavior

To evaluate the bioactivity behavior of the coatings, the samples were immersed in 100 ml of SBF solution in a plastic tube and kept at 37 ± 0.5°C for 3 weeks. The detailed description of the bioactivity behavior can be found in ref. [11].

3. RESULTS AND DISCUSSIONS

3.1. Voltage-time responses

The voltage-time response of the coatings without and with Mg_2SiO_4 NPs and their corresponding breakdown and final voltages (V_b and V_f, respectively), are shown in Fig. 2. Regardless of the presence of NPs in the electrolyte, both voltage-time plots followed a similar trend and possessed three different regions. At the initial stage, a very thin insulating layer of MgO formed on the surface of the Mg anode and voltage ascended linearly. In the second stage, voltage rose at a much lower rate than stage one. In this stage, which is called the micro-arc stage, the degradation of vulnerable parts of the MgO film happened and white transient sparks emerged on the anode surface, which contributed to uniform film thickening. Finally, in stage 3, the coating became thicker and the number of weak sites decreased, so the breakdown became more complicated and the voltage gradually reached a stable state. In this stage, sparks became more intense, but their number diminished. After adding of Mg_2SiO_4 NPs into the electrolyte, both V_b and V_f increased from 429 to 456 V and 433 to 467 V, respectively. Moreover, the time to gain the V_b increased from ~ 50 to 70 s with the addition of Mg_2SiO_4 NPs. This showed that the formation of the barrier layer could be retarded by the Mg_2SiO_4 NPs in the electrolyte. Under the action of an electrical field and mechanical stirring, Mg_2SiO_4 NPs with a negative zeta potential of −32.40 mV could easily move to the electrolyte/ coating interface of the anode. Then, the electrolyte/ coating interface adsorbed Mg_2SiO_4 particles, which increased the resistance of the coating and further increased the required voltage to overcome the resistance of the coating to induce sparks. Moreover, since a larger V_f leads to a thicker coating [34], it can be noted that the Mg_2SiO_4 NPs raised the coating growth rate.
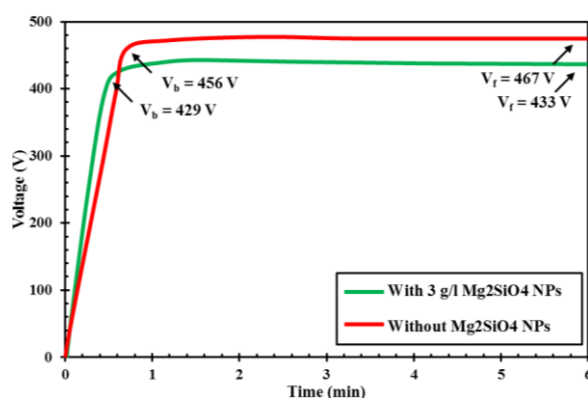

Fig. 2. Voltage-time plots of coatings prepared using electrolytes without and with Mg_2SiO_4 NPs.

Table 1. The chemical composition of SBF solution

NaCl	NaHCO₃	KCl	K₂HPO₄.3H₂O	MgCl₂.6H₂O	1 (mol/l)-HCl	CaCl₂	Na₂SO₄	Tris
8.035 g/l	0.355 g/l	0.225 g/l	0.231 g/l	0.311 g/l	39 ml/l	0.292 g/l	0.072 g/l	6.118 g/l

Amirhossein Kazemi, Arash Fattah-alhosseini, Maryam Molaei, Meisam Nouri

3.2. Microstructure and elemental analysis of coatings

Surface morphologies and EDS spectra of coatings prepared in electrolytes without and with Mg_2SiO_4 NPs are shown in Fig. 3. The EDS results are listed in Table 2. Both coatings displayed porous structures and had many micropores and some microcracks. During the PEO process, sparks cause the eruption of melted substances from discharge channels and form micropores on the coating surface [35].

The microcracks are also produced owing to the thermal stresses resulting from the quick solidification of molten materials [36]. Although the size and number of defects were similar for both coatings, for the coating with Mg_2SiO_4 NPs a lot of small white particles (indicated by yellow arrows) were adhered to the surface and inside the pores indicating that NPs might take part in PEO processing. Based on the EDS analysis, both coatings were composed of Mg, Na, O, P, and Ca elements and for the coating with Mg_2SiO_4 NPs, Si was also present in the result. The Na, O, P, Si and Ca originated from the electrolytes and the Mg and O were attributed to the MgO layer

formed during the PEO process. The presence of Si in the coating having Mg_2SiO_4 NPs indicated that particles were incorporated into the coatings successfully.

The EDS elemental mapping of coatings in Fig. 4 demonstrated the uniform distribution of all elements (Na, Mg, Na, Ca, P and Si) on the surface of the coatings, confirming the uniform composition of coatings. Cross-sectional micrographs of coatings are presented in Fig. 5. After adding Mg_2SiO_4 NPs into the electrolyte, the thickness of coating was increased from 19.40 ± 1.25 to 25.47 ± 1.62 μm. As mentioned before, the thicker nature of the coating with Mg_2SiO_4 NPs was corresponded to the higher V_f recorded for its electrolyte during the PEO process.
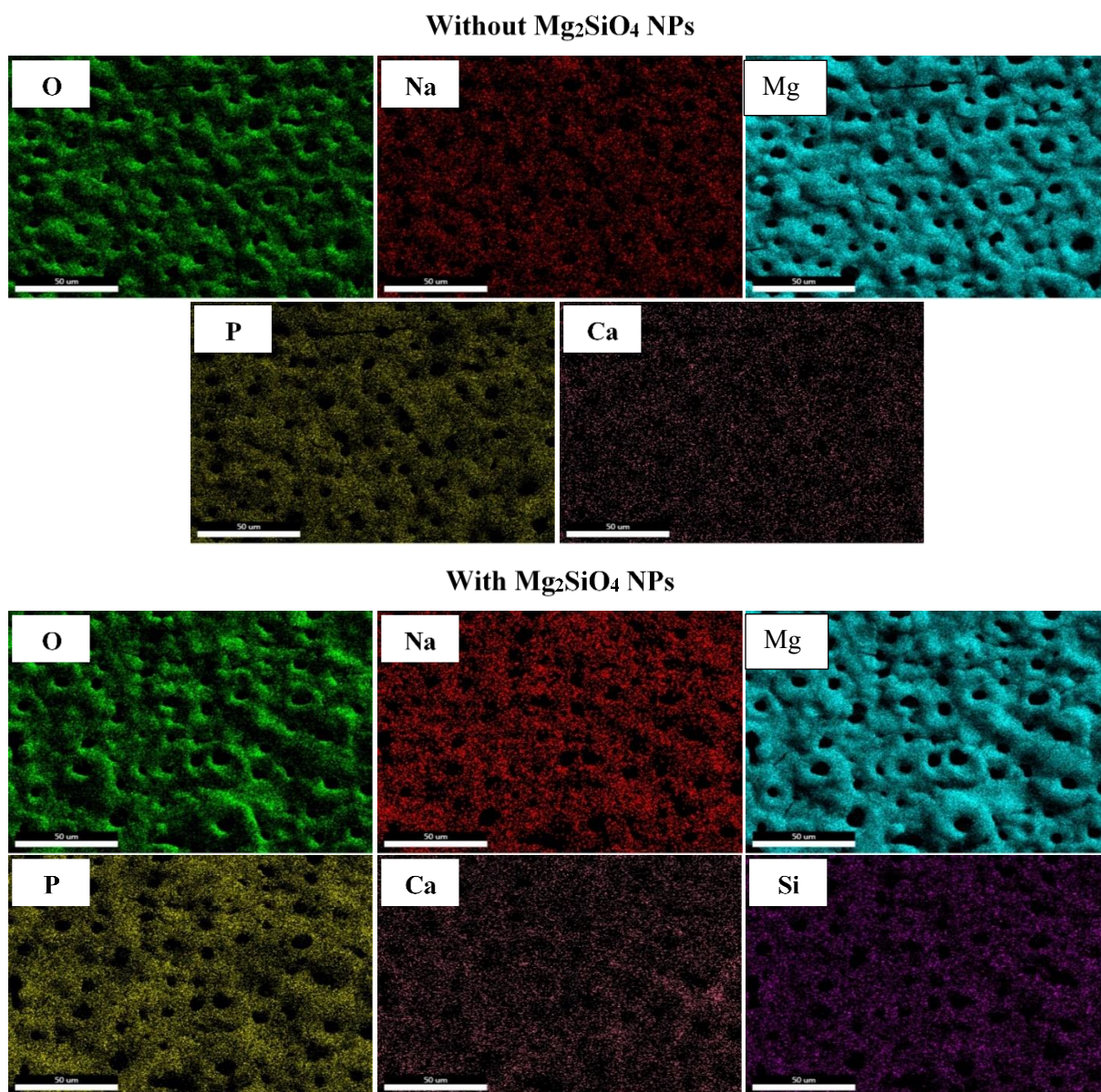
3.3. Phase analysis of coatings

The results of XRD for coatings with and without Mg_2SiO_4 NPs are presented in Fig. 6. CaP, MgO and $Mg_3(PO_4)_2$ phases were available in both coatings. During the PEO process, crystalline MgO and $Mg_3(PO_4)_2$ oxides are formed owing to the high pressure and temperature in the discharge channels because of the reaction of Mg^{2+} with O^{2-} or PO_4^{3-} anions [37–40].
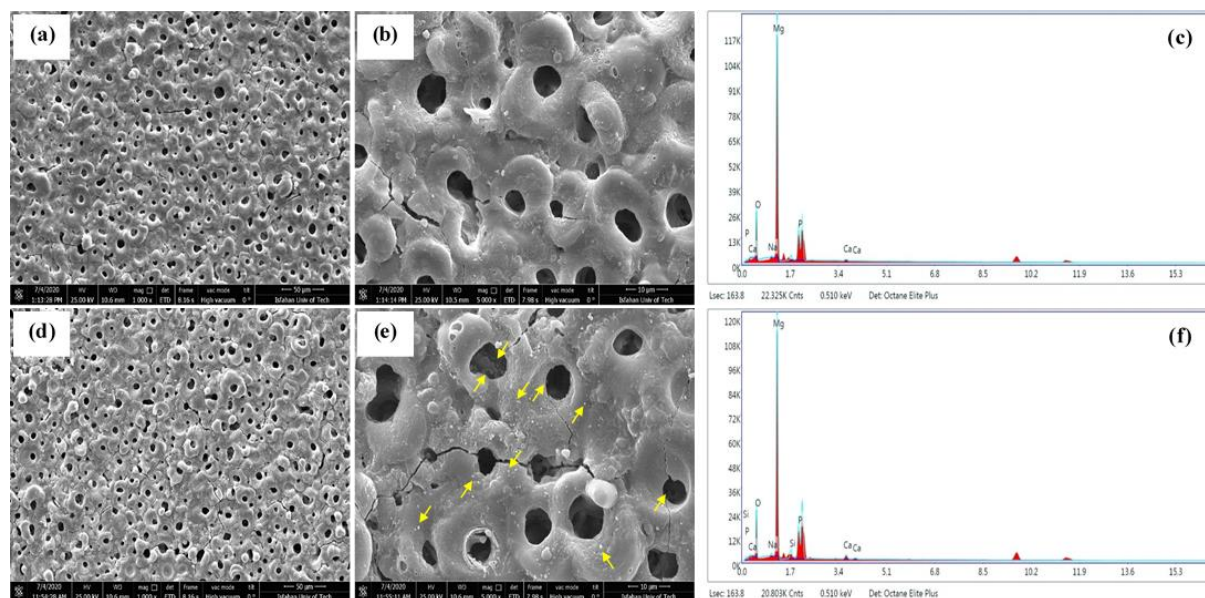

Fig. 3. The FE-SEM micrographs at magnifications of 1000x and 5000x and EDS local analysis of the coatings: (a, b, c) without Mg_2SiO_4 NPs and (d, e, f) with Mg_2SiO_4 NPs.

Table 2. The EDS results for coatings without and with Mg_2SiO_4 NPs

Coatings	Elements (at. %)						Ca/P ratio
	O	Na	Mg	P	Ca	Si	
Without Mg_2SiO_4 NPs	35.15	0.03	53.27	11.03	0.53	-	0.04
With Mg_2SiO_4 NPs	35.47	0.48	49.48	11.34	0.63	2.60	0.05

Without Mg$_2$SiO$_4$ NPs

With Mg$_2$SiO$_4$ NPs

Fig. 4. The EDS elemental mapping analysis of the surface of coatings without and with Mg$_2$SiO$_4$ NPs.
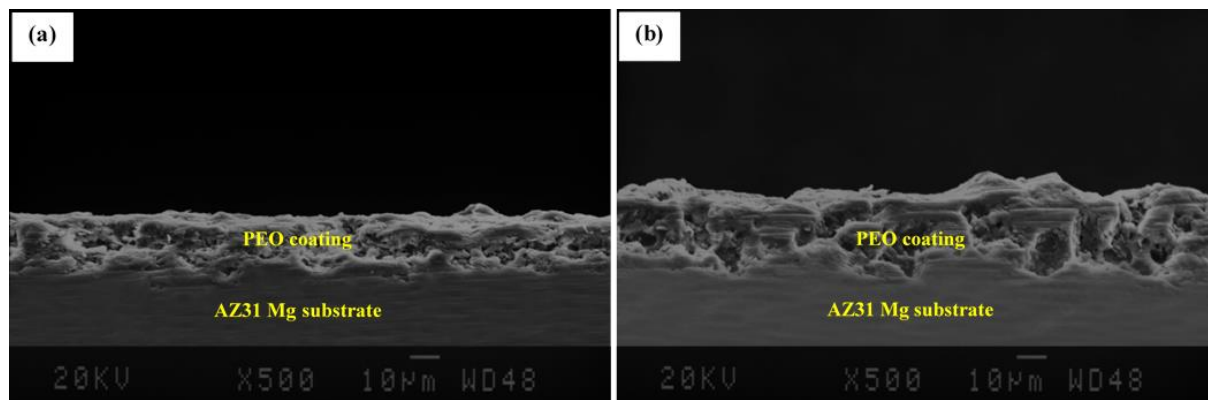
Fig. 5. The SEM cross-sectional morphology images at a magnification of 500x of coatings: (a) without Mg$_2$SiO$_4$ NPs and (b) with Mg$_2$SiO$_4$ NPs.

Amirhossein Kazemi, Arash Fattah-alhosseini, Maryam Molaei, Meisam Nouri

The intensities of MgO and $Mg_3(PO_4)_2$ peaks decreased by the addition of Mg_2SiO_4 NPs in the electrolyte. Despite the presence of Si in EDS, no diffraction peak related to the Mg_2SiO_4 particles was detected in the coating with NPs. The main reason might be the low content of the particles in the coating. In addition, there were some peaks related to elemental Mg that came from the substrates due to the thin nature of the coatings.

To study the participation of Mg_2SiO_4 NPs in the coating, FT-IR analysis was performed on the coating with Mg_2SiO_4 NPs and the result is indicated in Fig. 7. The corresponding PO_4^{3-} group peaks appeared at 622 and 1029 cm^{-1} due to the use of a phosphate-based electrolyte in the coating process [41]. The characteristic peak at about 800 cm^{-1} was related to the symmetric stretching vibration mode of Si−O−Si [7, 42, 43] confirming the Mg_2SiO_4 NPs were introduced into the coating successfully. The broad peaks between 1300-1755 and 2800-3800 cm^{-1} were assigned to the bending vibrations of H−O−H and stretching vibrations of O−H bonding of hydroxyl (OH$^-$) of water molecules absorbed on the surface of the coating, respectively [5, 44, 45]. OH$^-$ groups can form intramolecular or intermolecular H_2 bonding, resulting in peak widening [46].
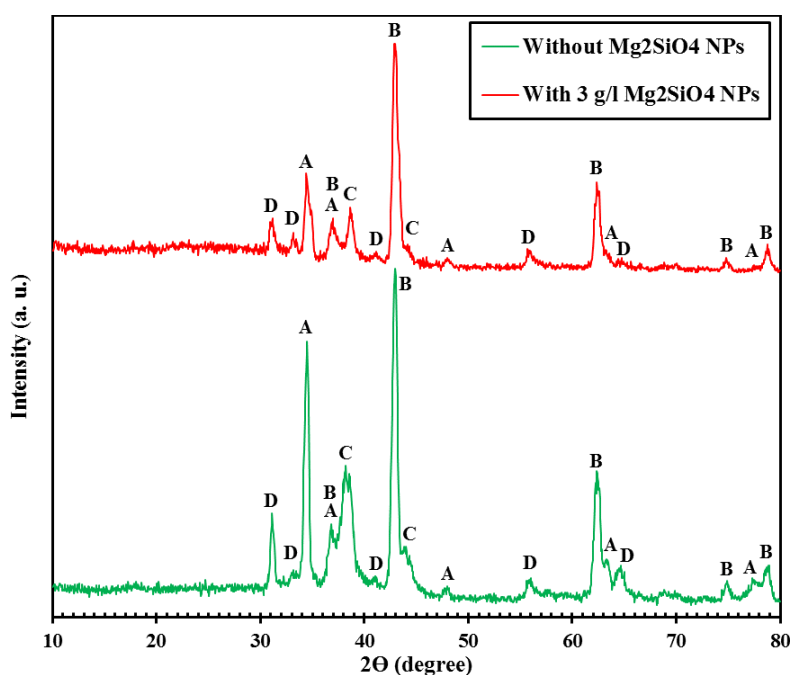

Fig. 6. The XRD patterns of coatings without and with Mg_2SiO_4 NPs.
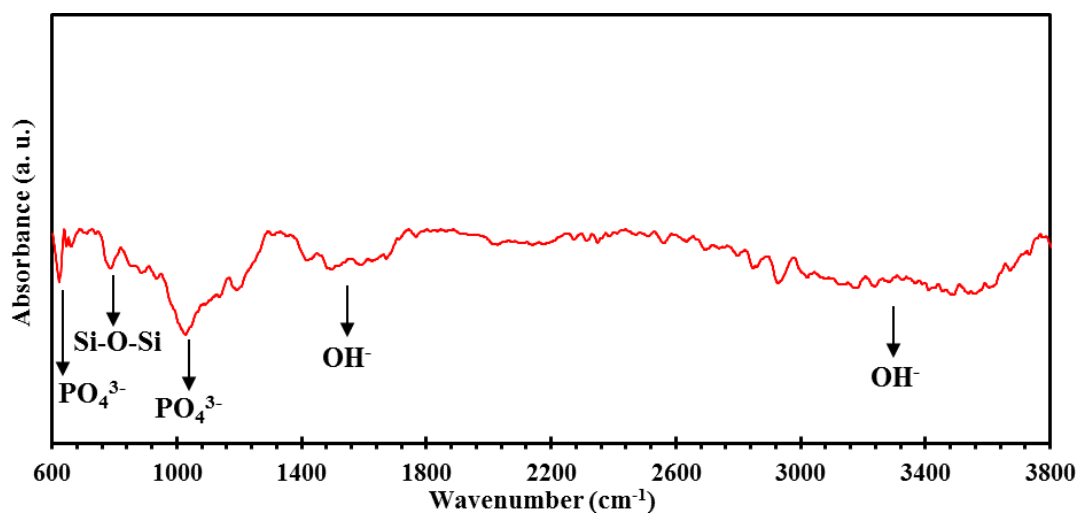

Fig. 7. The FT-IR spectra of coating with Mg_2SiO_4 NPs.

6

3.4. Wettability and surface roughness of coatings

The average surface roughness (R_a) values for coatings without and with Mg_2SiO_4 NPs were measured at 1.60 ± 0.06 and 1.48 ± 0.05 μm, respectively. After adding Mg_2SiO_4 NPs into the electrolyte, the R_a value of the coating did not change significantly. Fig. 8 presents the result of the wettability test and the measured water contact angles for the coatings without and with Mg_2SiO_4 NPs. As can be seen, the coating without Mg_2SiO_4 NPs showed a smaller water contact angle ($\Theta \sim 83.8° \pm 3.2$) and, therefore, a better wettability than the coating with Mg_2SiO_4 NPs ($\Theta \sim 104.1° \pm 1.1$). The wettability of PEO coatings is influenced by the chemical composition of the coatings and the geometry of the surfaces [47].
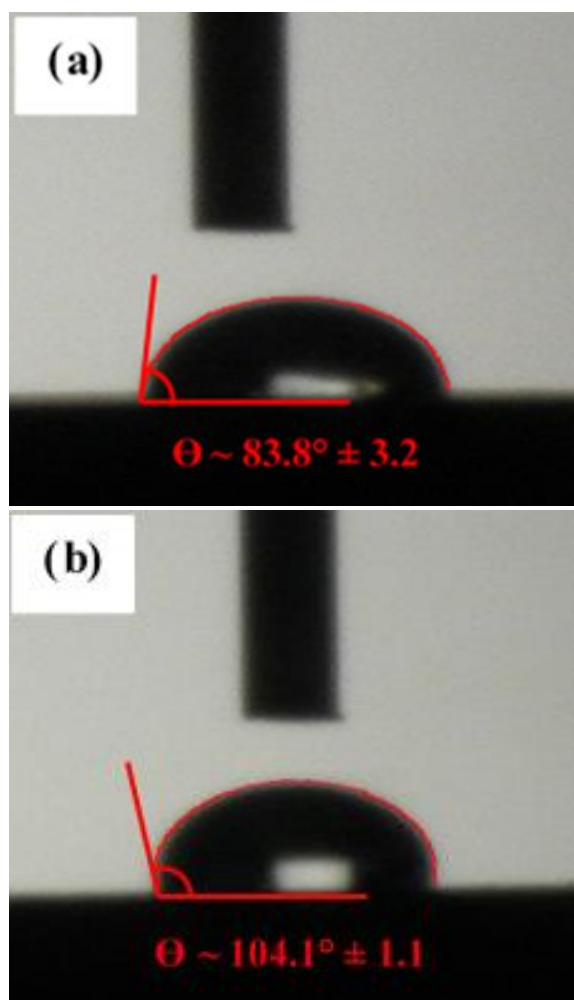
Fig. 8. The microscopic images of the wettability test along with calculated contact angles for coatings: (a) without Mg_2SiO_4 NPs and (b) with Mg_2SiO_4 NPs.

Since the MgO phase can absorb OH^- groups and raise the wettability of PEO coatings on Mg substrates [32], the higher content of MgO in the coating without Mg_2SiO_4 NPs was the main reason for the better wettability of this coating. Therefore, the composition of coatings was the main factor affecting their wettability.

### 3.5. Corrosion behavior of coatings

3.5.1. EIS measurements

The Nyquist and Bode plots of coatings prepared in electrolytes without and with Mg_2SiO_4 NPs after exposure to SBF solution for different durations are presented in Fig. 9. Nyquist plots for both coatings at all exposure times (Fig. 9 (a, c, e, g)) included two high-frequency (10 to 100000 Hz) and low-frequency (0.01 to 10 Hz) capacitive loops. Since the structure of PEO coatings includes two porous outer and compact inner layers, the existence of the two loops in Nyquist plots is caused by a change in oxide coatings behavior. At all exposure times, the Bode plots (Fig. 9 (b, d, f, h)) demonstrated high to medium and low- frequency regions.

In the former region, a linear relationship was identified between frequency and absolute impedance which demonstrated a coating/solution interface with capacitive behavior. The impedance module was almost constant in the latter region. The equivalent electrical circuit used for modeling Nyquist plots is shown in Fig. 10. The fitted data are shown by solid lines in Fig. 9 and the results are summarized in Table 3.

In the simulated circuit in Fig. 10, R_s, R_o, and R_i correspond to the SBF solution, outer PEO layer, and inner PEO layer resistances, respectively. Also, this circuit includes two constant phase elements: CPE_o and CPE_i which are related to the outer and the inner films of the PEO coatings, respectively. CPE represents a simple capacitor that simulates the heterogeneity of the surface and diffusion factors [48]. The following equation expresses the impedance of CPE [49]:

$$Z_{CPE}= 1/[Y_0(j\omega)^n] \qquad (1)$$

Where Y_0 shows the constant of CPE, ω indicates the angular frequency (1 rad/s), j denotes the imaginary unit, and n is the constant that ranges between 0 and 1 [49, 50]. Up to 3 days, the coating with Mg_2SiO_4 NPs possessed a lower corrosion resistance ($R_o + R_i$) than the coating without Mg_2SiO_4 NPs, but the behavior was reversed after 1 week.

Amirhossein Kazemi, Arash Fattah-alhosseini, Maryam Molaei, Meisam Nouri
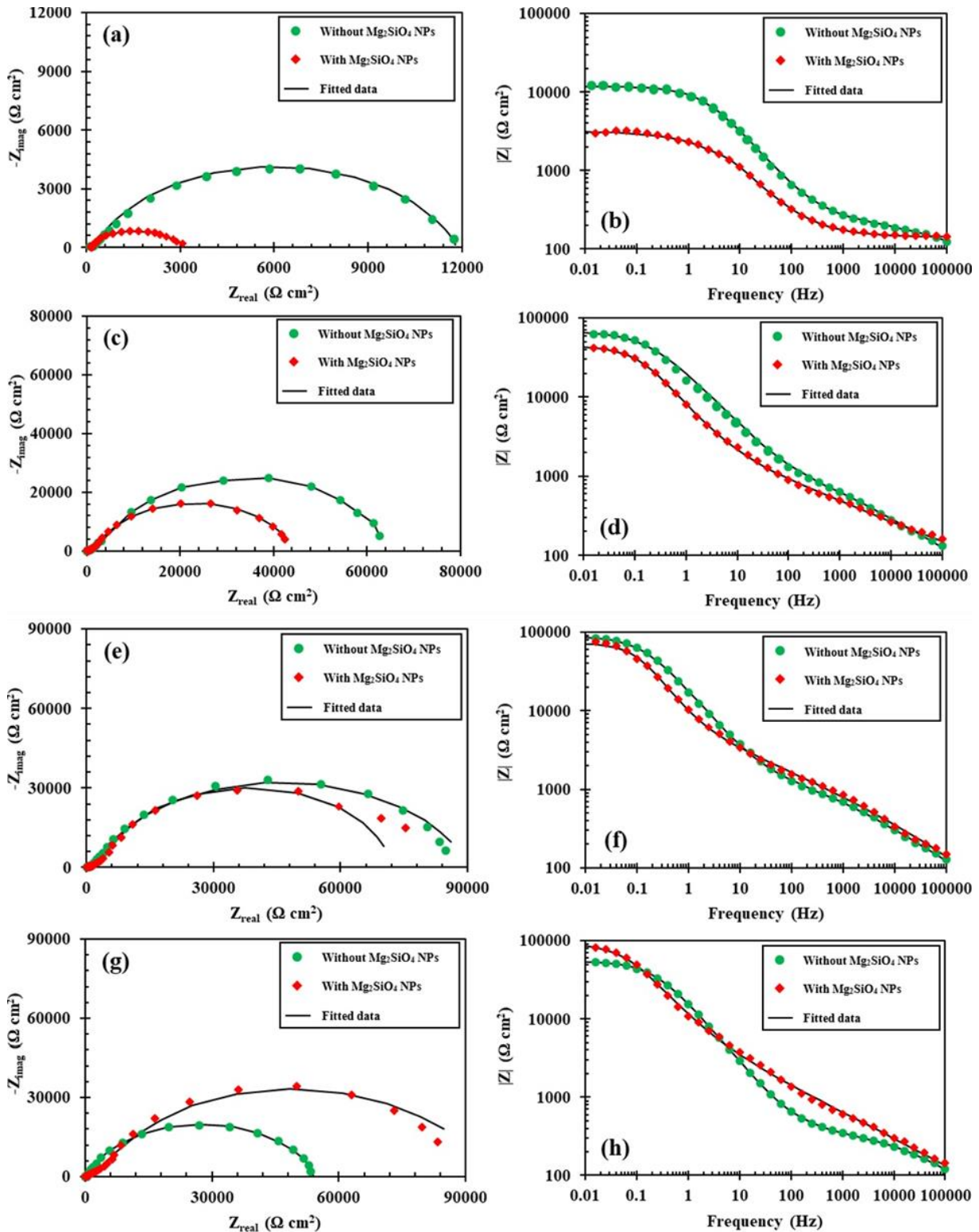
Fig. 9. Nyquist and Bode plots of coatings exposed to SBF solutions for periods of (a, b) 1 hour, (c, d) 1 day, (e, f) 3 days, and (g, h) 1 week.

After 1 week, while the corrosion resistance of the coating without Mg_2SiO_4 NPs dropped from 69.59 to 42.89 $k\Omega$ cm^2, the resistance of coating with Mg_2SiO_4 NPs increased from 63.48 to 71.29 $k\Omega$ cm^2. With the incorporation of Mg_2SiO_4 NPs into the coating, the corrosion resistance was

8

increased about 1.66 times. The enhanced corrosion resistance of coating with Mg_2SiO_4 NPs over time was related to the preventing role of the corrosion products layer formed over the surface of the coating. In fact, during the exposure to SBF, decomposition of the Mg_2SiO_4 can form negative silanol groups $(Si-OH^-)$ through the reaction of the hydration products of Mg_2SiO_4 with H_2O which in turn can electrostatically absorb Ca^{2+} and PO_4^{3-} ions from the SBF [51–54]. Meanwhile, the reduced corrosion resistance of coating without Mg_2SiO_4 NPs after 1 week was because of the insufficient protection of corrosion products layer against Cl^- corrosive ions diffusion.

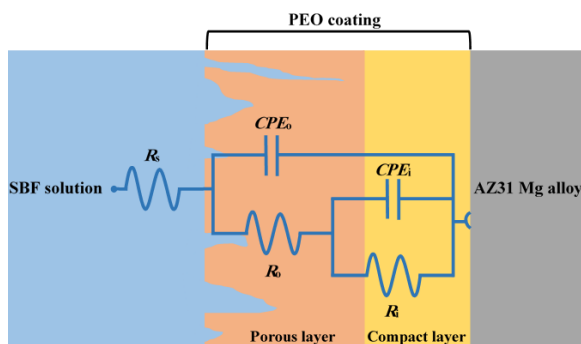**Fig. 11.** PDP plots of coatings after exposure to SBF solution for 1 week.

Fig. 10. The equivalent circuit used for modeling the Nyquist plots of coatings.

3.5.2. PDP measurements

Fig. 11 shows the PDP curves of PEO coatings prepared in electrolytes without and with Mg_2SiO_4 NPs after exposure for 1 week to SBF. In addition, the electrochemical data and polarization resistance (R_p) of the coatings are listed in Table 4. The R_p values were determined through the approximate linear polarization at the E_{corr} from the following equation [55]:

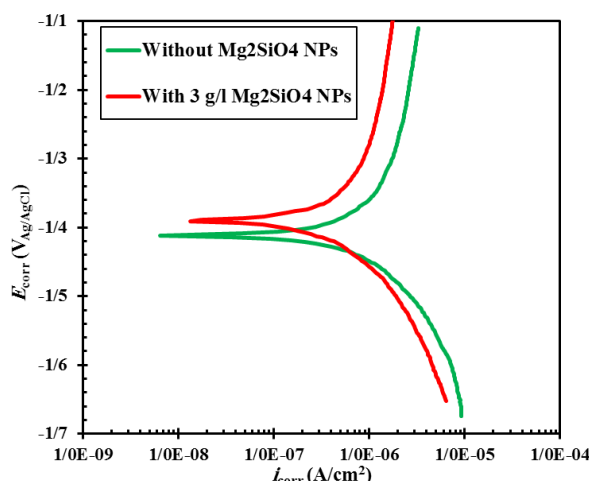$$R_p = \beta_a\beta_c/2.303(\beta_a+\beta_c)i_{corr} \tag{2}$$

While the E_{corr} values were almost similar for both coatings (about -1.41 and -1.39 V for coatings without and with Mg_2SiO_4 NPs, respectively), the coating with Mg_2SiO_4 NPs possessed the lower i_{corr} value (0.22 $\mu A/cm^2$) as compared with the coating without NPs (0.38 $\mu A/cm^2$). In this way, the calculated R_p value of the coating with NPs (12.30 $k\Omega$ cm^2) was higher more than 2 times than that of the coating without NPs (5.58 $k\Omega$ cm^2). Generally, a thicker coating provides better insulation between the corrosion solution and coating. Besides, the corrosion resistance of PEO coatings is governed by their wettability. Generally, greater wettability increases the susceptibility to corrosion [56, 57]. Therefore, the better corrosion protection of coating with Mg_2SiO_4 NPs was related to its greater thickness, lower wettability, and the presence of corrosion-resistant Mg_2SiO_4 particles inside the pores which increased the length of the diffusion path of Cl^- ions through the substrate.

Table 3. Results of the EIS test after exposure for different times to SBF

Exposure times	Coatings	n_o	CPE_o $(\mu F/cm^2)$	R_o $(K\Omega\ cm^2)$	n_i	CPE_i $(\mu F/cm^2)$	R_i $(K\Omega\ cm^2)$
1 hour	Without Mg_2SiO_4 NPs	0.28	14.00	0.20	0.90	17.84	10.31
	With Mg_2SiO_4 NPs	0.79	34.14	0.60	0.64	73.92	2.06
1 day	Without Mg_2SiO_4 NPs	0.42	26.21	0.58	0.70	11.89	54.82
	With Mg_2SiO_4 NPs	0.29	56.11	0.72	0.83	30.17	34.44
3 days	Without Mg_2SiO_4 NPs	0.43	21.78	0.77	0.79	12.63	68.82
	With Mg_2SiO_4 NPs	0.32	63.92	1.01	0.94	25.25	62.47
1 week	Without Mg_2SiO_4 NPs	0.41	16.22	0.24	0.80	13.04	42.65
	With Mg_2SiO_4 NPs	0.34	78.57	2.13	0.86	29.42	69.16

Amirhossein Kazemi, Arash Fattah-alhosseini, Maryam Molaei, Meisam Nouri

Table 4. Electrochemical data obtained from PDP test after exposure for 1week to SBF

| Coatings	E_{corr} ($V_{Ag/AgCl}$)	i_{corr} ($\mu A/cm^2$)	β_a (dec)	β_c (dec)	R_p ($k\Omega$ cm^2)
Without Mg_2SiO_4 NPs	-1.41	0.38	0.010	0.010	5.58
With Mg_2SiO_4 NPs	-1.39	0.22	0.012	0.014	12.30

3.5.3. Corrosion microstructure and elemental analysis of coatings

The surface morphologies of the coatings without and with Mg_2SiO_4 NPs after exposure for 1 week to SBF solution are shown in Fig. 12. The EDS results are given in Table 5. There were no corrosion pits and delamination on either of the coatings' surfaces, showing good corrosion resistance of PEO coatings. Most surface micropores and microcracks of the coatings were disappeared due to the precipitated corrosion products layer. Since SBF is a highly supersaturated solution that enables the formation of Ca- and P-containing compounds [58, 59], these precipitates on the surface of the coatings were probably the Ca-P compounds. Based on the EDS analysis, in both coatings O, Na, Mg, P, Cl, and Ca elements were detected. Moreover, Si was still present on the surface of the coating with Mg_2SiO_4 NPs. The presence of Cl in the coatings revealed that the Cl^- species of SBF were involved in the corrosion processes.

The results of EDS elemental mapping analysis on the surface of the coatings exposed to SBF for 1 week are shown in Fig. 13. All elements were distributed evenly over the surface of the coatings.

However, it seems Ca was accumulated in some regions. The more colorful Ca and P maps compared to those before exposure to SBF were related to the formation of calcium-phosphate compounds on the surfaces of the coatings.
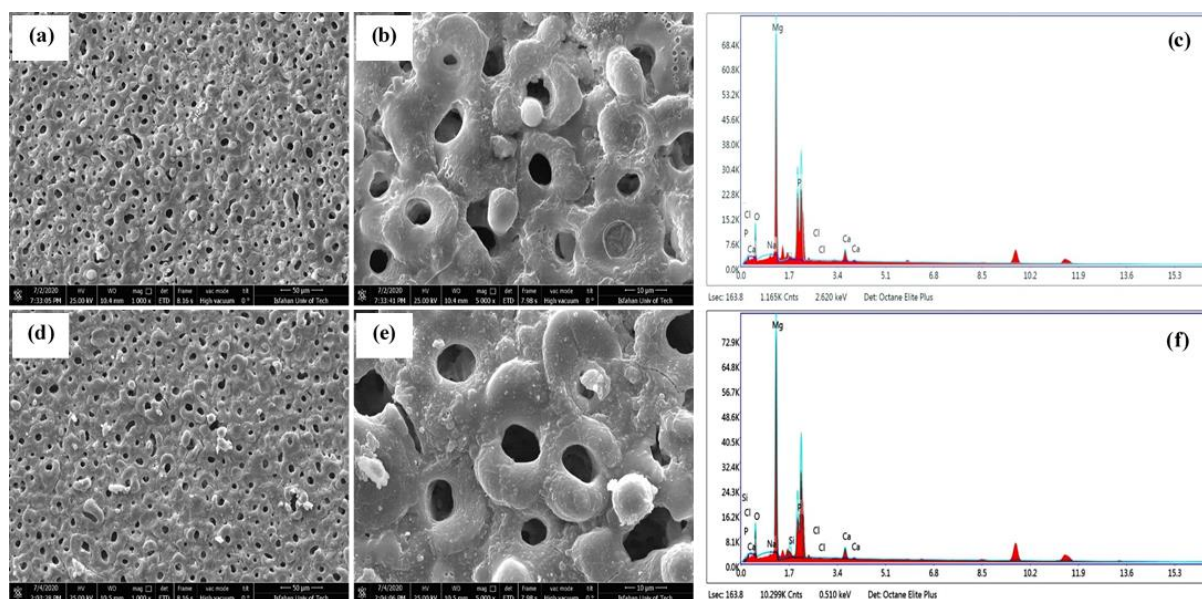
Fig. 12. The FE-SEM micrographs at two magnifications of 1000x and 5000x with EDS local analysis after exposure to SBF solution for 1 week for the coatings (a, b, c) without Mg_2SiO_4 NPs and (d, e, f) with Mg_2SiO_4 NPs.

Table 5. The EDS results for coatings without and with Mg_2SiO_4 NPs after exposure to SBF solutions for 1 week

Coatings	Elements (at. %)							Ca/P ratio
	O	Na	Mg	P	Cl	Ca	Si	
Without Mg_2SiO_4 NPs	28.10	0.00	46.11	22.35	0.04	3.40	-	0.15
With Mg_2SiO_4 NPs	27.46	0.00	47.45	17.94	0.03	3.51	3.61	0.19

10
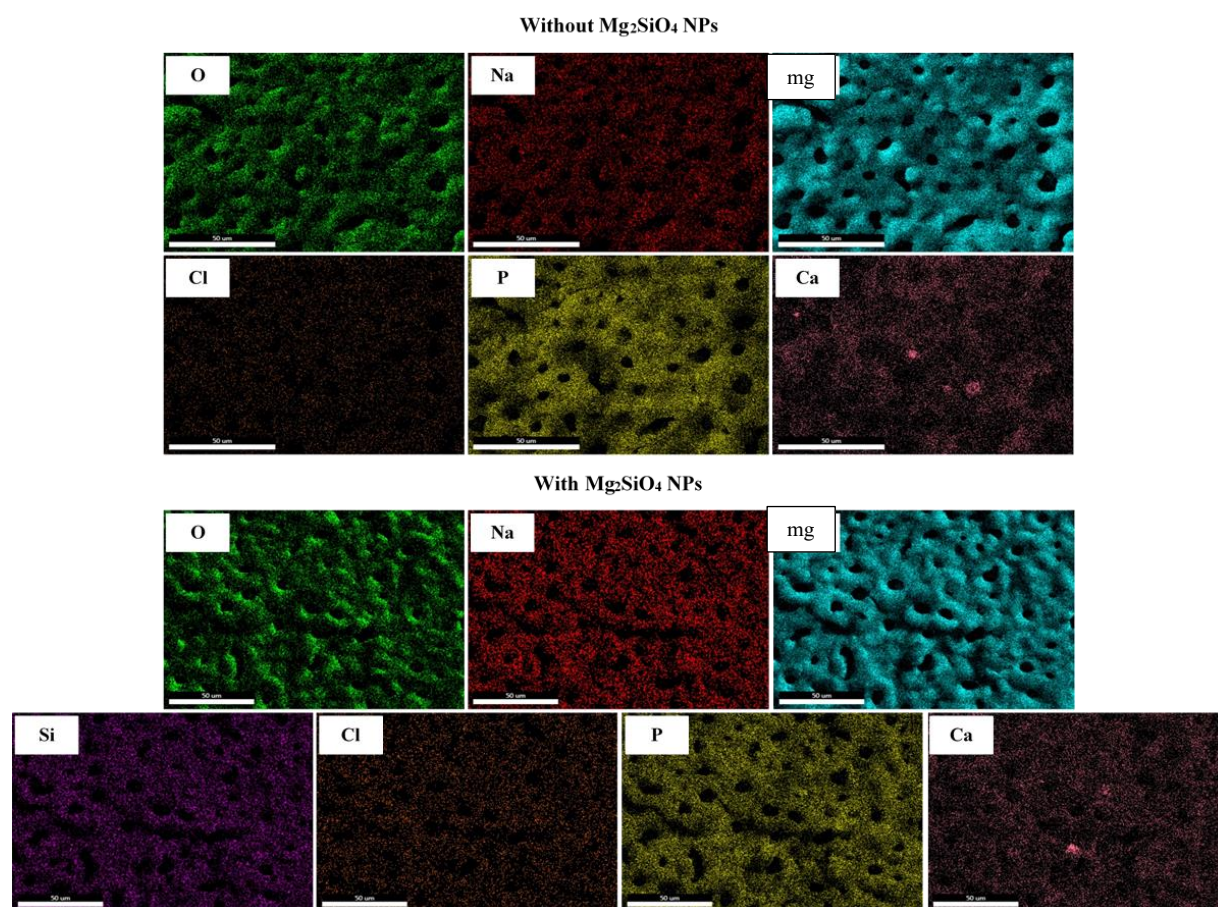
Fig. 13. The surface EDS elemental mapping analysis of the surface of coatings without and with Mg_2SiO_4 NPs after exposure to SBF solution for 1 week.

3.6. In-vitro bioactivity behavior of coatings

Surface micrographs and EDS local analysis of the PEO coatings without and with Mg_2SiO_4 NPs after 3 weeks of immersion in SBF solution are presented in Fig. 14. Moreover, the EDS results are summarized in Table 6. As can be seen, while the whole surface of the coating without Mg_2SiO_4 NPs was surrounded by an even apatite layer, some apatite-like particles randomly scattered on the surface of the coating with Mg_2SiO_4 NPs. Therefore, it seems that the coating with NPs possessed a less apatite formation ability and as a result, weaker bioactivity property than the coating without NPs.

In addition, in both coatings, numerous cracks were observed on the surface resulting from corrosion reaction during the immersion in SBF. The EDS results revealed that the Ca/P ratios of the coatings without and with Mg_2SiO_4 NPs were 1.17 and 0.92 at. %, respectively. The Ca/P ratio of both coatings was less than the stoichiometric Ca/P ratio of 1.67 at. % for hydroxyapatite which its chemical structure is similar to both tooth minerals and natural bone tissues [60]. This indicated that the formed apatite on coatings surfaces was Ca deficient HA. The low Ca/P ratio of coatings might be due to the high content of P species in the electrolytes. The more remarkable apatite forming ability of the coating without Mg_2SiO_4 NPs could be attributed to its higher wettability which encouraged ion exchange and in turn, amplified the apatite growth [32].

4. CONCLUSIONS

This study investigated the role of Forsterite (Mg_2SiO_4) nanoparticles (NPs) incorporation on the corrosion and bioactivity behavior of the as-prepared calcium-phosphate PEO coating on AZ31 alloy. The main results can be summarized as follows:

11
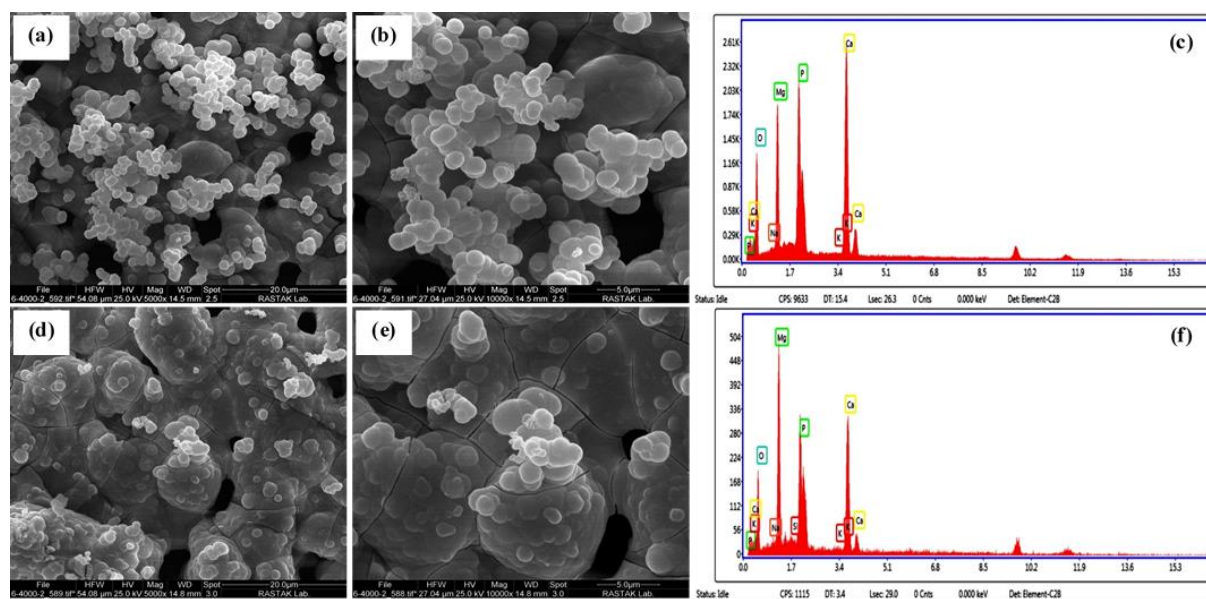
Fig. 14. The FE-SEM micrographs at two magnifications of 5000x and 10000x with EDS local analysis after immersing for 3 weeks in SBF solution for the coatings: (a, b, c) without Mg₂SiO₄ NPs and (d, e, f) with Mg₂SiO₄ NPs.

Table 6. The EDS results for coatings without and with Mg₂SiO₄ NPs after immersion for 3 weeks in SBF

Coatings	Elements (at. %)							Ca/P ratio
	O	Na	Mg	P	K	Ca	Si	
Without Mg$_2$SiO$_4$ NPs	55.42	1.73	16.15	12.27	0.06	14.37	-	1.17
With Mg$_2$SiO$_4$ NPs	48.30	2.43	22.68	12.68	0.23	11.68	2.00	0.92

1. Although both coatings without and with Mg$_2$SiO$_4$ NPs displayed porous structure with micropores and microcracks, in the coating with Mg$_2$SiO$_4$ NPs many tiny particles adhered to the surface and inside the pores. Moreover, by adding Mg$_2$SiO$_4$ NPs to the electrolyte, the thickness of the coating layer increased.

2. According to XRD patterns, both coatings included MgO, Mg$_3$(PO$_4$)$_2$, and CaP phases. Although no peaks associated with Mg$_2$SiO$_4$ were observed in the XRD pattern of coating with NPs, the FT-IR spectra revealed the Si−O−Si band which confirmed the incorporation of the Mg$_2$SiO$_4$ NPs in the coating.

3. After adding of Mg$_2$SiO$_4$ NPs into the base electrolyte, although the surface roughness of coating did not change significantly, its wettability decreased.

4. The polarization resistance (R$_P$) of the coating having Mg$_2$SiO$_4$ NPs after 1 week of exposure to simulated body fluid (SBF) was obtained as 12.30 kΩ cm^2 which was higher more than 2 times than that of the coating without Mg$_2$SiO$_4$ NPs (with R$_p$ of 5.58 kΩ cm^2). This was because of the thicker coating layer, lower wettability, and presence of Mg$_2$SiO$_4$ NPs inside the pores for the coating with Mg$_2$SiO$_4$ NPs.

5. After immersion for 3 weeks in SBF, the ability of the surface to form apatite for the coating with Mg$_2$SiO$_4$ NPs decreased. This was attributed to the lower wettability of coating with Mg$_2$SiO$_4$ particles. After 3 weeks, the calculated Ca/P ratios of the coatings without and with Mg$_2$SiO$_4$ NPs were 1.17 and 0.92 at. %, respectively.

REFERENCES

[1] Wu, Y. Wang, Y. Tian, S. Li, H. Zhao, Y. Jia, D. Zhou, Y. "Formation mechanism, degradation behavior, and cytocompatibility of a double-layered structural MAO/ rGO-CaP coating on AZ31 Mg." Colloids Surfaces B Biointerfaces. 2020, 190 110901.

[2] Chaharmahali, R. Fattah-alhosseini, A. Babaei, K. "Improving surface characteristics of PEO coatings of Mg and its alloys with zirconia nanoparticles: a review." Appl. Surf. Sci. Adv. 2021, 5, 100131.

[3] Tang, Y. Zhu, L. Zhang, P. Zhao, K. Wu, Z. "Enhanced corrosion resistance of bio-piezoelectric composite coatings on medical magnesium alloys." Corros. Sci. 2020, 176, 108939.

[4] Fattah-alhosseini, A. Molaei, M. Nouri, M. Babaei, K. "Antibacterial activity of bioceramic coatings on Mg and its alloys created by plasma electrolytic oxidation (PEO): A review." J. Magnes. Alloy. 2022, 10, 81–96.

[5] Molaei, M. Fattah-alhosseini, A. Babaei, K. "Improving the wear resistance of plasma electrolytic oxidation (PEO) coatings applied on Mg and its alloys under the addition of nano- and micro-sized additives into the electrolytes: A review." J. Magnes. Alloy. 20212, 9. 1164–1186.

[6] Vakili-Azghandi, M. Fattah-alhosseini, A. "Effects of Duty Cycle, Current Frequency, and Current Density on Corrosion Behavior of the Plasma Electrolytic Oxidation Coatings on 6061 Al Alloy in Artificial Seawater." Metall. Mater. Trans. A Phys. Metall. Mater. Sci. 2017, 48, 4681–4692.

[7] Chaharmahali, R. Fattah-alhosseini, A. Babaei, K. "Surface characterization and corrosion behavior of calcium phosphate (Ca-P) base composite layer on Mg and its alloys using plasma electrolytic oxidation (PEO): A review." J. Magnes. Alloy. 2021, 9, 21-40.

[8] Chaharmahali, R. Fattah-Alhosseini, A. Esfahani, H. "Increasing the in-vitro corrosion resistance of AZ31B-Mg alloy via coating with hydroxyapatite using plasma electrolytic oxidation." J. Asian Ceram. Soc. 2020, 8, 39–49.

[9] Wierzbicka, E. Vaghefinazari, B. Lamaka, S. V. Zheludkevich, M.L. Mohedano, M. Moreno, L. Visser, P. Rodriguez, A. Velasco, J. Arrabal, E. Matykina, R. "Flash-PEO as an alternative to chromate conversion coatings for corrosion protection of Mg alloy." Corros. Sci. 2021, 180, 109189.

[10] Fattah-alhosseini, A. Chaharmahali, R. Keshavarz, M.K. Babaei, K. "Surface characterization of bioceramic coatings on Zr and its alloys using plasma electrolytic oxidation (PEO): A review." Surf. Interfaces. 2021, 25, 101283.

[11] Nikoomanzari, E. Fattah-alhosseini, A. Pajohi Alamoti, M.R. Keshavarz, M.K."Effect of ZrO$_2$ nanoparticles addition to PEO coatings on Ti-6Al-4V substrate: microstructural analysis, corrosion behavior and antibacterial effect of coatings in Hank's physiological solution." Ceram. Int., 2020, 46, 13114-13124.

[12] Roknian, M. Fattah-alhosseini, A. Gasht, S. O. "Plasma Electrolytic Oxidation Coatings on Pure Ti Substrate: effects of Na$_3$PO$_4$ concentration on morphology and corrosion behavior of coatings in Ringer's physiological solution." J. Mater. Eng. Perform. 2018, 27, 1343–1351.

[13] Fattah-alhosseini, A. Molaei, M. Babaei, K. "The effects of nano- and micro-particles on properties of plasma electrolytic oxidation (PEO) coatings applied on titanium substrates: A review." Surf. Interfaces. 2020, 21, 100659.

[14] Fattah-alhosseini, A. Chaharmahali, R. Babaei, K. "Effect of particles addition to solution of plasma electrolytic oxidation (PEO) on the properties of PEO coatings formed on magnesium and its alloys: A review." J. Magnes. Alloy. 2020, 8, 799–818.

[15] Atapour, M. Blawert, C. Zheludkevich, M.L. "The wear characteristics of CeO$_2$ containing nanocomposite coating made by aluminate-based PEO on AM 50 magnesium alloy." Surf. Coat. Technol. 2019, 357, 626–637.

[16] Wang, P. Gong, Z.Y. Hu, J. Pu, J. Cao, W.J. "Effect of MgO micro-powder on the characteristics of micro-arc oxidation coatings." Surf. Eng. 2019, 35, 627–634.

[17] Jia, L. Liang, C. Huang, N. Duan, F. Wang, L. "Formation of Hydroxyapatite produced by Microarc oxidation coupled with sol-gel technology." Mater. Manuf. Process. 2014, 29, 1085–1094.

[18] Salami, B. Afshar, A. Mazaheri, A. "The

effect of sodium silicate concentration on microstructure and corrosion properties of MAO-coated magnesium alloy AZ31 in simulated body fluid." J. Magnes. Alloy. 2014, 2, 72–77.

[19] Razavi, M. Fathi, M. Savabi, O. Vashaee, D. Tayebi, L. "In Vitro Analysis of Electrophoretic Deposited Fluoridated Hydroxyapatite Coating on Micro-arc Oxidized AZ91 Magnesium Alloy for Biomaterials Applications." Metall. Mater. Trans. A Phys. Metall. Mater. Sci. 2015, 46, 1394–1404.

[20] Razavi, M. Fathi, M. Savabi, O. Vashaee, D. Tayebi, L. "In vivo assessments of bioabsorbable AZ91 magnesium implants coated with nanostructured fluoridated hydroxyapatite by MAO/EPD technique for biomedical applications." Mater. Sci. Eng. C. 2015, 48, 21–27.

[21] Aktug, S.L. Durdu, S. Aktas, S. Yalcin, E. Usta, M. "Surface and in vitro properties of Ag-deposited antibacterial and bioactive coatings on AZ31 Mg alloy." Surf. Coat. Technol. 2019, 375, 46–53.

[22] Lee, H.P. Lin, D.J. Yeh, M. L. "Phenolic modified ceramic coating on biodegradable Mg alloy: The improved corrosion resistance and osteoblast-like cell activity." Materials (Basel). 2017, 10,696.

[23] Lee, J. Kim, Y. Chung, W. "Effect of Ar bubbling during plasma electrolytic oxidation of AZ31B magnesium alloy in silicate electrolyte." Appl. Surf. Sci. 2012, 259, 454–459.

[24] Zhang, L. Zhang, J. Chen, C. Gu, Y. "Advances in microarc oxidation coated AZ31 Mg alloys for biomedical applications." Corros. Sci. 2015, 91, 7–28.

[25] Zhang, Y. Chen, F. Zhang, Y. Du, C. "Influence of graphene oxide additive on the tribological and electrochemical corrosion properties of a PEO coating prepared on AZ31 magnesium alloy." Tribol. Int. 2020, 146, 106135.

[26] Zhu, Y. Zhang, S. Zhao, R. Lou, J. Zhang, R. Huan, X. Zhang, Y. "Influences of Na_2SiO_3 and $EDTA-ZnNa_2$ concentration on properties of zinc-containing coatings on WE43 magnesium alloys." Surf. Coat. Technol. 2018, 356, 108–122.

[27] Hua, Y. Zhang, Z. Li, W. "Microstructure and degradation properties of C-containing composite coatings on magnesium alloy wires treated with micro-arc oxidation." Surf. Coat. Technol. 2016, 291, 70–78.

[28] Wang, Y. Huang, Z. Yan, Q. Liu, C. Liu, P. Zhang, Y. Guo, C. Jiang, G. Shen, D. "Corrosion behaviors and effects of corrosion products of plasma electrolytic oxidation coated AZ31 magnesium alloy under the salt spray corrosion test." Appl. Surf. Sci. 2016, 378, 435–442.

[29] Ur Rehman, Z. Koo, B.H. "Effect of $Na_2SiO_3 \cdot 5H_2O$ concentration on the microstructure and corrosion properties of two-step PEO coatings formed on AZ91 alloy." Surf. Coat. Technol. 2017, 317, 117–124.

[30] Ryu, H.S. Hong, S.-H. "Corrosion Resistance and Antibacterial Properties of Ag-Containing MAO Coatings on AZ31 Magnesium Alloy Formed by Microarc Oxidation." J. Electrochem. Soc. 2010, 157, C131.

[31] Razavi, M. Biodegradation, "Bioactivity and In vivo Biocompatibility Analysis of Plasma Electrolytic Oxidized (PEO) Biodegradable Mg Implants." Phys. Sci. Int. J. 2014, 4, 708–722.

[32] Attarzadeh, N. Kazemi, A. Molaei, M. Fattah-alhosseini, A. "Multipurpose surface modification of PEO coatings using tricalcium phosphate addition to improve the bedding for apatite compounds." J. Alloys Compd. 2021, 877, 160275.

[33] Kokubo, T. Takadama, H. "How useful is SBF in predicting in vivo bone bioactivity?" Biomaterials. 2006, 27, 2907–2915.

[34] Shen, D. Ma, H. Guo, C. Cai, J. Li, G. He, D. Yang, Q. "Effect of cerium and lanthanum additives on plasma electrolytic oxidation of AZ31 magnesium alloy." J. Rare Earths. 2013, 31, 1208–1213.

[35] Molaei, M. Fattah-Alhosseini, A. Gashti, S.O. "Sodium Aluminate Concentration Effects on Microstructure and Corrosion Behavior of the Plasma Electrolytic Oxidation Coatings on Pure Titanium." Metall. Mater. Trans. A Phys. Metall. Mater. Sci. 2018, 49, 368–375.

[36] Babaei, K. Fattah-alhosseini, A. Molaei, M. "The effects of carbon-based additives

on corrosion and wear properties of Plasma electrolytic oxidation (PEO) coatings applied on Aluminum and its alloys : A review." Surf. Interfaces. 2020, 21, 100677.

[37] Zhu, F. Wang, J. Li, S. Zhang, J. "Preparation and characterization of anodic films on AZ31B Mg alloy formed in the silicate electrolytes with ethylene glycol oligomers as additives." Appl. Surf. Sci. 2012, 258, 8985–8990.

[38] Lai Liu, L. Xia Yang, P. Na Su, C. Fei Guo, H. Zhong An, M. "Microstructure and corrosion behavior of micro-arc oxidation film on magnesium alloy." Int. J. Electrochem. Sci. 2013, 8, 6077–6084.

[39] Wu, Y.F. Wang, Y.M. Jing, Y.B. Zhuang, J.P. Yan, J.L. Shao, Z.K. Jin, M.S. Wu, C.J. Zhou, Y. "In vivo study of microarc oxidation coated biodegradable magnesium plate to heal bone fracture defect of 3 mm width." Colloids Surfaces B Biointerfaces. 2017, 158, 147–156.

[40] Chen, H. Lv, G.H. Zhang, G.L. Pang, H. Wang, X.Q. Lee, H.J. Yang, S.Z. "Corrosion performance of plasma electrolytic oxidized AZ31 magnesium alloy in silicate solutions with different additives." Surf. Coat. Technol. 2010, 205, S32-S35.

[41] M.Rúa, J. Zuleta, A.A. Ramírez, J. Fernández-Morales, P. "Micro-arc oxidation coating on porous magnesium foam and its potential biomedical applications." Surf. Coat. Technol. 2019, 360, 213–221.

[42] Ge, Y. Jiang, B. Yang, Z. Li, Y. "Microstructure and corrosion resistance behavior of composite micro-arc oxidation and SiO_2 coatings on magnesium alloys." Adv. Mater. Res. 2011, 160–162, 1834–1838.

[43] Wang, S. Guo, X. Xie, Y. Liu, L. Yang, H. Zhu, R. Gong, J. Peng, L. Ding, W. "Preparation of superhydrophobic silica film on Mg-Nd-Zn-Zr magnesium alloy with enhanced corrosion resistance by combining micro-arc oxidation and sol-gel method." Surf. Coat. Technol. 2012, 213, 192–201.

[44] Bordbar-Khiabani, A. Yarmand, B. Sharifi-Asl, M. Mozafari, S. "Improved corrosion performance of biodegradable magnesium in simulated inflammatory condition via drug-loaded plasma electrolytic oxidation coatings." Mater. Chem. Phys. 2020, 239, 122003.

[45] Cao, G. Wang, L. Fu, Z. Hu, J. Guan, S. Zhang, C. Wang, L. Zhu, S. "Chemically anchoring of TiO_2 coating on OH-terminated $Mg_3(PO_3)_2$ surface and its influence on the in vitro degradation resistance of Mg-Zn-Ca alloy." Appl. Surf. Sci. 2014, 308, 38–42.

[46] Gao, H. Zhang, M. Yang, X. Huang, P. Xu, K. "Effect of Na_2SiO_3 solution concentration of micro-arc oxidation process on lap-shear strength of adhesive-bonded magnesium alloys." Appl. Surf. Sci. 2014, 314 447–452.

[47] Hariprasad, S. Gowtham, S. Arun, S. Ashok, M. Rameshbabu, N. "Fabrication of duplex coatings on biodegradable AZ31 magnesium alloy by integrating cerium conversion (CC) and plasma electrolytic oxidation (PEO) processes." J. Alloys Compd. 2017, 722, 698–715.

[48] Bala Srinivasan, P. Liang, J. Blawert, C. Störmer, M. Dietzel, W. "Effect of current density on the microstructure and corrosion behaviour of plasma electrolytic oxidation treated AM50 magnesium alloy." Appl. Surf. Sci. 2009, 255, 4212–4218.

[49] Hussein, R.O. Zhang, P. Nie, X. Xia, Y. Northwood, D.O. "The effect of current mode and discharge type on the corrosion resistance of plasma electrolytic oxidation (PEO) coated magnesium alloy AJ62." Surf. Coat. Technol. 2011, 206, 1990–1997.

[50] Hussein, R.O. Northwood, D.O. Nie, X. "The effect of processing parameters and substrate composition on the corrosion resistance of plasma electrolytic oxidation (PEO) coated magnesium alloys." Surf. Coat. Technol. 2013, 237, 357–368.

[51] Razavi, M. Fathi, M. Savabi, O. Vashaee, D. Tayebi, L. "In vitro study of nanostructured diopside coating on Mg alloy orthopedic implants." Mater. Sci. Eng. C. 2014, 41, 168–177.

[52] Seyfoori, A. Mirdamadi, S. Mehrjoo, M. Khavandi, A. "In-vitro assessments of micro arc oxidized ceramic films on AZ31

Amirhossein Kazemi, Arash Fattah-alhosseini, Maryam Molaei, Meisam Nouri

magnesium implant: Degradation and cell-surface response." Prog. Nat. Sci. Mater. Int. 2013, 23, 425–433.

[53] Seyfoori, A. Mirdamadi, S. Khavandi, A. Raufi, Z.S. "Biodegradation behavior of micro-arc oxidized AZ31 magnesium alloys formed in two different electrolytes." Appl. Surf. Sci. 2012, 261, 92–100.

[54] Dou, J. Zhao, Y. Lu, L. Gu, G. Yu, H. Chen, C. "Effect of the second-step voltages on the structural and corrosion properties of silicon-calcium-phosphate (Si-CaP) coatings on Mg-Zn-Ca alloy." R. Soc. Open Sci. 2018, 5, 172410.

[55] Ma, Y. Hu, H. Northwood, D. Nie, X. "Optimization of the electrolytic plasma oxidation processes for corrosion protection of magnesium alloy AM50 using the Taguchi method." J. Mater. Process. Technol. 2007, 182, 58–64.

[56] Asgari, M. Aliofkhazraei, M. Darband, G.B. Rouhaghdam, A.S. "Evaluation of alumina nanoparticles concentration and stirring rate on wear and corrosion behavior of nanocomposite PEO coating on AZ31 magnesium alloy." Surf. Coat. Technol. 2017, 309, 124–135.

[57] Guo, J. Wang, L. Wang, S.C. Liang, J. Xue, Q. Yan, F. "Preparation and performance of a novel multifunctional plasma electrolytic oxidation composite coating formed on magnesium alloy." J. Mater. Sci. 2009, 44, 1998–2006.

[58] Bordbar-Khiabani, A. Yarmand, M. Mozafari, B. "Enhanced corrosion resistance and in-vitro biodegradation of plasma electrolytic oxidation coatings prepared on AZ91 Mg alloy using ZnO nanoparticles-incorporated electrolyte." Surf. Coat. Technol. 2019, 360, 153–171.

[59] Narayanan, T.S.N.S. Lee, M.H. "A simple strategy to modify the porous structure of plasma electrolytic oxidation coatings on magnesium." RSC Adv. 2016, 6, 16100–16114.

[60] Xiong, Y. Hu, X. Weng, Z. Song, R. "Stress Corrosion Resistance of Laser Shock Peening/Microarc Oxidation Reconstruction Layer Fabricated on AZ80 Magnesium Alloy in Simulated Body Fluid." J. Mater. Eng. Perform. 2020, 29, 5750–5756.

16